

This is the accepted manuscript made available via CHORUS. The article has been published as:

Lattice dynamics in the FeSb_3 skutterudite

A. Möchel, I. Sergueev, N. Nguyen, Gary J. Long, Fernande Grandjean, D. C. Johnson, and
R. P. Hermann

Phys. Rev. B **84**, 064302 — Published 19 August 2011

DOI: [10.1103/PhysRevB.84.064302](https://doi.org/10.1103/PhysRevB.84.064302)

Lattice Dynamics in the FeSb₃ Skutterudite

A. Möchel,^{1,2} I. Sergueev,³ N. Nguyen,⁴ Gary J. Long,⁵
Fernande Grandjean,² D. C. Johnson,⁴ and R. P. Hermann^{1,2,*}

¹Jülich Centre for Neutron Science JCNS and Peter Grünberg Institut PGI,
JARA-FIT, Forschungszentrum Jülich GmbH, D-52425 Jülich, Germany

²Faculté des Sciences, Université de Liège, B-4000 Liège, Belgium

³European Synchrotron Radiation Facility, F-38043 Grenoble Cedex, France

⁴Department of Chemistry and Materials Science Institute, University of Oregon, Eugene, OR 97403, USA

⁵Department of Chemistry, Missouri University of Science and Technology,
University of Missouri, Rolla, Missouri 65409-0010, USA

(Dated: July 5, 2011)

Thin films of FeSb₃ were characterized by electronic transport, magnetometry, x-ray diffraction, ⁵⁷Fe and ¹²¹Sb nuclear inelastic scattering, and ⁵⁷Fe Mössbauer spectroscopy. Resistivity and magnetometry measurements reveal semiconducting behavior with a 16.3(4) meV band gap and an effective paramagnetic moment of 0.57(6) μ_B , respectively. A systematic comparison of the lattice dynamics with CoSb₃ and EuFe₄Sb₁₂ reveals that the [Fe₄Sb₁₂] framework is softer than the [Co₄Sb₁₂] framework, and that the observed softening and the associated lowering of the lattice thermal conductivity in the RFe₄Sb₁₂ filled skutterudites is not only related to the filler but also to the [Fe₄Sb₁₂] framework.

PACS numbers: 63.20.D-, 76.80.+y, 72.20.Pa, 61.05.C-, 65.40.Ba, 65.40.De

I. INTRODUCTION

Skutterudites are promising thermoelectric materials that have been intensively studied since the 1990s¹⁻⁴. They possess interesting semiconducting properties, notably a large Seebeck coefficient, and a relatively low thermal conductivity that has been ascribed to the dynamics of the filler⁵⁻⁷. In particular the lattice dynamics of filled and unfilled skutterudites has been the object of intensive research⁸⁻¹². The semiconducting, magnetic, and thermal properties of the filled $R(\text{Fe,Co})_4\text{Sb}_{12}$ skutterudites can be tuned^{6,13} by filling the $(\text{Fe,Co})_4\text{Sb}_{12}$ framework with monovalent ions, *e.g.*, Na⁺ and Tl⁺, divalent ions, *e.g.*, Yb²⁺ and Eu²⁺, or trivalent ions, *e.g.*, La³⁺ and Ce³⁺. However, only a limited degree of filling can be achieved^{6,13,14} in CoSb₃. In order to achieve larger degrees of filling either Co must be substituted by Fe or a synthesis involving ball milling and subsequent hot pressing must be used¹⁵.

Because there is no successful bulk synthesis procedure, the influence of filling the FeSb₃ structure on its lattice dynamics has been studied by different approaches. The direct comparison with the lattice dynamics of the [Fe₄Sb₁₂] polyanion is not possible, thus one approach is the comparison^{9,10} of the lattice dynamics of the filled structures mentioned above with the related unfilled CoSb₃. Another approach is the study of the contribution of the filler R to the density of phonon states (DPS). Density functional theory calculations of the partial density of phonon states have been carried out and compared with experimental data, obtained by inelastic neutron scattering and nuclear inelastic scattering^{16,17}. The partial contributions to the DPS can also be investigated by *ab initio* powder-averaged lattice dynamic calculations and a subsequent comparison with inelastic

neutron scattering measurements¹¹.

The synthesis of FeSb₃ is however possible by nanoalloying^{18,19} and this approach has recently been improved and now yields higher sample purity, but still produces only small amounts in the form of micrometer thick films. Because detailed knowledge of the lattice dynamics in skutterudites is necessary to unravel the mechanisms that yield their low thermal conductivity, characterization methods suitable for thin films have to be used. Although inelastic neutron scattering experiments are in principle feasible, the beamtime required would be prohibitively long because of the small amount of sample. In contrast, nuclear inelastic scattering (NIS) is a method of choice that yields the DPS for selected elements²⁰ even with small samples. This method has been applied²¹ to the ⁵⁷Fe nuclear resonance for some time, and has recently been developed¹⁷ for the ¹²¹Sb resonance. The resolution for the latter isotope was recently improved²² to ~ 1.3 meV full width at half maximum (FWHM). It is thus possible to fully access the element specific DPS in FeSb₃ and to obtain several related quantities²⁰, such as the mean force constants, the atomic displacement parameters, and the average velocity of sound.

Herein we report both the macroscopic characterization of high purity FeSb₃ by resistivity and susceptibility measurements and the microscopic characterization by synchrotron radiation diffraction, ⁵⁷Fe Mössbauer spectral measurements, and nuclear inelastic scattering by ⁵⁷Fe and ¹²¹Sb. A comparison of these results with the properties of CoSb₃ reveals that FeSb₃ is significantly softer, an observation that both reveals a combined influence of the filler and the substitution of Fe for Co on the lattice dynamics and hence thermal properties, and

provides additional clues to the low thermal conductivity in filled skutterudites.

II. EXPERIMENTAL

The FeSb_3 thin films were deposited on Kapton foil at ambient temperature by the elemental modulated reactant method in a custom-built ultra high vacuum, $\approx 10^{-5}$ Pa, deposition system described elsewhere²³. Fe was deposited by using a 3 kW electron beam gun at a rate of 0.4 Å/s and Sb was deposited by using an effusion cell at a rate of 0.6 Å/s. A computer was used to control the deposition procedure. A quartz crystal monitoring system placed 25 cm above each source was used to control the elemental layer modulation, the deposition rates, the shutter opening time for Fe, and the thickness for Sb. The precursors for the crystallized films were prepared by depositing multiple alternate layers of Fe and Sb until the desired film thickness was obtained. Deposition parameters were determined to yield the appropriate molar stoichiometry of FeSb_3 . These precursor films were then annealed under a nitrogen atmosphere at 410 K to form FeSb_3 . With this method, two films of thicknesses of ~ 1 and ~ 1.5 μm were deposited on a 25 μm thick Kapton substrate. All further measurements were carried out on these two films.

Temperature dependent resistivity and magnetization measurements were carried out between 10 and 300 K on a physical properties measurement system (QD-PPMS) with the resistivity and the vibrating sample magnetometer option. **The resistivity was measured on several 1 μm thick samples with 2 by 5 mm^2 lateral dimension and different microcrack structures by the 4-point method.** The magnetization measurements were carried out with an applied magnetic induction of 0.25 T on a 80 cm by 3.7 mm long wrapped ribbon of the 1 μm thick film, *i.e.*, ~ 12.9 mg of FeSb_3 . Hysteresis measurements have been carried out at 300 K up to 1.5 T in order to assess the presence of impurity phases and the diamagnetic contribution to the susceptibility. The same measurements have been carried out on polycrystalline CoSb_3 for comparison. The susceptibility, χ , was calculated from the magnetization by assuming the validity of the low field limit approximation $\chi = M/H$, where M is the magnetization and H the applied field.

Temperature dependent x-ray diffraction measurements were carried out at the 6-ID-D high-energy station at the APS between 10 and 300 K. **The x-ray wavelength was 0.124269 Å, and the sample - area detector distance was 1601.1(1) mm, as determined with a NIST SRM640c Si standard. Silicon (Chempur, 99.999%) was used as an internal standard for the temperature calibration.** The sample contained 10 layers of a ~ 1.5 μm thick film of FeSb_3 on Kapton foil and, for better thermal coupling to the sample holder, Al foil was placed between each layer. The powder diffraction pattern of CoSb_3 was measured under the same conditions. The data were reduced to

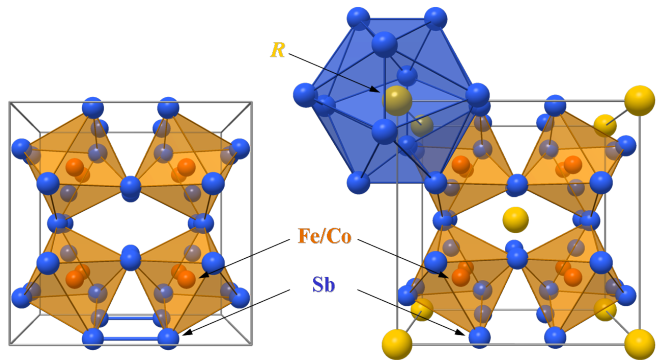


FIG. 1. The structure of unfilled CoSb_3 or FeSb_3 (left) and filled $R\text{Fe}_4\text{Sb}_{12}$ (right) skutterudite. Co or Fe, Sb, and R are shown in red, blue, and yellow, respectively. The blue rectangle indicates one of the Sb rings, see text.

diffraction patterns by using Fit2D²⁴ and analyzed using the Rietveld method²⁵.

The ^{57}Fe Mössbauer spectra have been measured between 4.2 and 295 K on a constant-acceleration spectrometer that utilized a 295 K rhodium matrix ^{57}Co source and was calibrated at 295 K with α -Fe powder.

The ^{121}Sb NIS by FeSb_3 was measured at the ID22N station at the ESRF operating in 16-bunch mode. A resolution of 1.3 meV was achieved by using a high resolution backscattering monochromator with the (8 16 $\bar{24}$ 40) reflection of a sapphire single crystal cooled to ~ 237 K. The sample containing 6 layers of a ~ 1.5 μm thick film of FeSb_3 on Kapton foil with Al foil between each layer was cooled to 25 K in order to minimize multiphonon scattering. The ^{121}Sb NIS of CoSb_3 and $\text{EuFe}_4\text{Sb}_{12}$ was measured on powder samples with the same setup and resolution. The 295 K ^{57}Fe NIS on the same FeSb_3 sample was measured at the ID18 station at the ESRF operating in 16 bunch mode with a resolution of 0.7 meV.

III. RESULTS AND DISCUSSION

A. Electric transport and magnetism

Above ~ 40 K the electrical resistivity, ρ_{el} , of FeSb_3 decreases with increasing temperature, see Fig. 2, a decrease that is indicative of semiconducting behavior. A fit of the data in high temperature region, see inset in Fig. 2, with $\rho_{el}(T) = A \cdot \exp(E_g/2k_B T)$, where E_g is the energy gap, k_B the Boltzmann constant, T the temperature, and A a proportionality constant, yields an electronic band gap of 16.3(4) meV, a narrower gap than the 50 meV gap obtained by resistivity measurements²⁶ on lightly *p*-doped CoSb_3 . As expected for rather thin films, the microstructure was found to be very important and resistivity measurements were carried out on several samples. **The smallest cracks or scratches will increase the resistivity by several orders of magnitude**

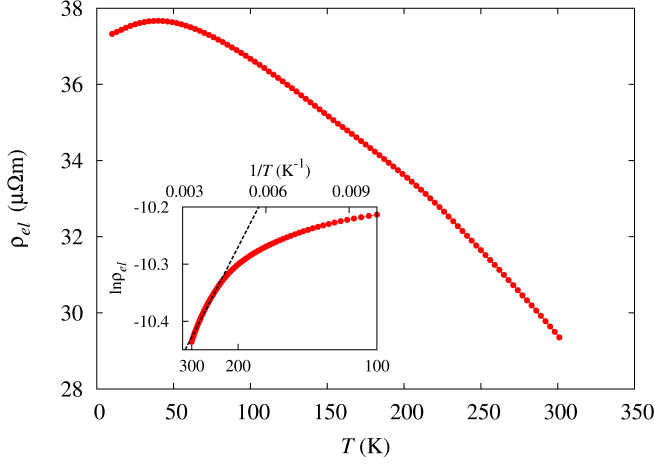


FIG. 2. Electrical resistivity, ρ_{el} , of FeSb₃ obtained between 10 and 300 K on a crack free sample, the errors are the size of the data points. The inset shows the fit between 220 and 300 K that yields an energy gap of 16.3(4) meV, see text.

with respect to pristine samples. Further, heating the sample above 300 K, not shown, induces additional microstructure and increases the resistivity, because of the differential thermal expansion between Kapton and FeSb₃. Atomic force microscopy measurements were carried out to monitor this behavior and to assure that the results in Fig. 2 were obtained on a sample free of cracks at the ~ 50 nm level. Such a dependence of the resistivity on the microstructure has also been observed²⁷ in polycrystalline CoSb₃, with reported resistivities of undoped samples between 7 and 1000 $\mu\Omega\text{m}$ at room temperature^{27–33}. The 300 K resistivity of 29.4(1) $\mu\Omega\text{m}$ observed for crack free FeSb₃ is similar to the 37 $\mu\Omega\text{m}$ of a polycrystalline, sintered, CoSb₃ sample³⁰, which also exhibits the temperature dependence of a typical semiconductor.

The molar susceptibilities, χ_m , of FeSb₃ and CoSb₃ are shown in Fig. 3. First, the diamagnetic contribution was obtained from the slope of a hysteresis loop measurement at 300 K, see Fig. 4, and is associated with the sample holder, the ion core diamagnetism, and, for the FeSb₃ films, to the Kapton substrate. The resulting corrections of χ_m^{dia} were assumed to be temperature independent and were used to obtain the results shown in Fig. 3. **Second, a small amount of soft ferromagnetic impurity in FeSb₃ was observed in the hysteresis loop, see Fig. 4, and this contribution was subtracted.** The magnetization of this impurity is essentially saturated at 0.25 T. Finally, a small correction term, χ_0 , amounting to $\sim 12\%$ of the diamagnetic correction was added to account for imperfections in the correction procedure. Adding this χ_0 immediately yielded paramagnetic Curie-Weiss behavior for FeSb₃ between 70 and 300 K. A plot of $1/\chi_m$, see Fig. 3, yields a Curie constant of 0.520(2) $\text{cm}^3\text{K/mol}$ with a 0 K Curie-Weiss temperature. The inset of Fig. 3 indicates that the

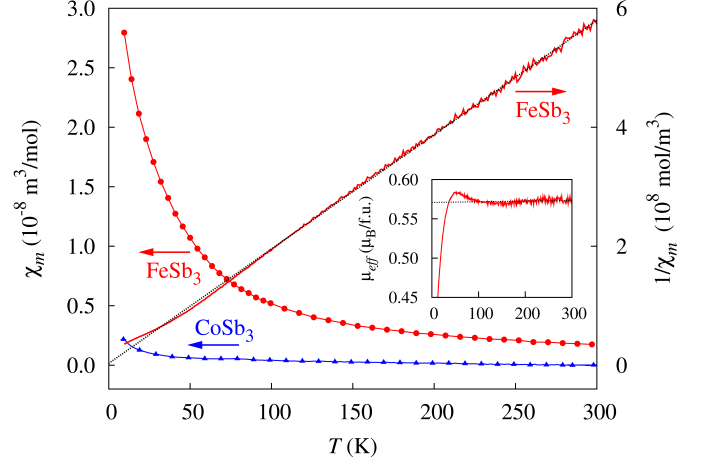


FIG. 3. The molar magnetic susceptibility and the inverse susceptibility obtained at 0.25 T between 10 and 300 K for FeSb₃ shown as circles (red), and the molar magnetic susceptibility for CoSb₃, triangles (blue), after corrections, see text. The errors are the size of the data points. Inset: the effective magnetic moment of FeSb₃.

effective paramagnetic moment of FeSb₃ of 0.57(6) μ_B per formula unit, obtained from $\mu_{eff} = 797.8 \cdot \sqrt{\chi_m \cdot T}$, is temperature independent above ~ 70 K. The same approach was used for CoSb₃ and an effective paramagnetic moment of 0.10(6) $\mu_B/\text{f.u.}$ was obtained, a value that is compatible with an earlier report³³. A study of $\text{Co}_{1-x}\text{Fe}_x\text{Sb}_3$ with x ranging from 0 to 0.1 has shown that μ_{eff} increases with increasing Fe content up to a maximum of 1.7 $\mu_B/\text{f.u.}$, a value that could correspond³² to low spin Fe^{3+} . This behavior obviously does not extrapolate to FeSb₃, which exhibits a much smaller effective paramagnetic moment.

From the y axis intercept of the magnetic hysteresis loop in Fig. 4 an impurity phase of 0.004(1) atom % was obtained by assuming a typical mean value of 2.2 μ_B per Fe impurity atom at room temperature. The coercive field of ~ 80 Oe indicates that the impurity phase is not elemental Fe. For CoSb₃ an elemental Co impurity phase of 0.0005(2) atom % was obtained by the same procedure.

B. X-ray diffraction

X-ray diffraction, see Fig. 5, indicates^{18,34} that both FeSb₃ and CoSb₃ form a cubic lattice with space group $\text{Im}\bar{3}$ (number 204) and have the skutterudite structure, see Fig. 1, where Fe or Co and Sb are located on the 8c and 24g sites, respectively. The inset to Fig. 5 shows the detector image with homogeneous Debye-Scherrer rings that indicate the absence of texture. **Apart from the Si internal standard, small traces of an impurity are observed visible as a shoulder at $2\theta \sim 2.3^\circ$ in Fig. 5, indicating a polycrystalline Sb impurity of less than 3 weight %.**

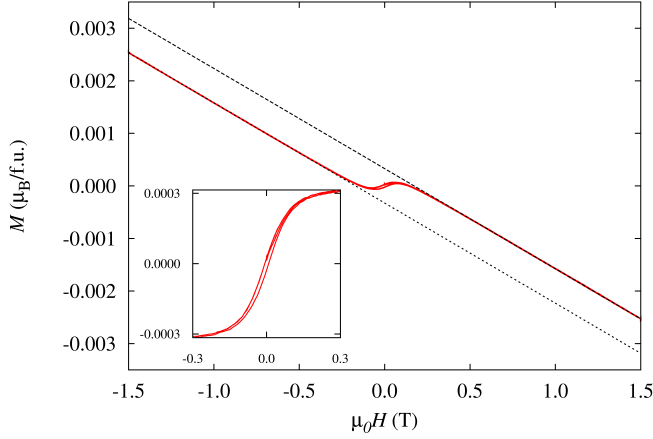


FIG. 4. Hysteresis loop of FeSb₃ measured at 300 K. The negative slope is indicative of diamagnetic behavior. The inset shows the hysteresis loop obtained after the diamagnetic correction discussed in the text.

No further phases nor the Al thermalization layers are observed. Because of the large background resulting from the 10 layers of Kapton foil, the Fourier filtering option was used to properly subtract the background, however even with this option the data below $2\theta = 2.1^\circ$ can not be refined because the background is too large and not monotonous. The parameters obtained at 10 and 300 K by Rietveld refinements are given in Table I. The Sb occupation was refined assuming full occupation of the Fe or Co site. The density obtained from the lattice parameters is also given in Table I. A temperature dependent diffraction study on CoSb₃ was carried out for comparison and the refinement parameters given in Table I are in good agreement with the literature values³⁴. From the refinement of the Sb occupation at 10 K a stoichiometry of FeSb_{2.88(5)} and CoSb_{2.97(3)} has been obtained. The corresponding 0.96(1) Sb occupancy in FeSb₃ is however problematic, see discussion in the Mössbauer spectroscopy section below.

A study of the Co_{1-x}Fe_xSb₃ solid solutions, with x between 0 and 0.1, reveals that their lattice parameters increase linearly with increasing Fe content, in agreement with Vegard's law³². If we assume that this linearity holds true for higher Fe content, a lattice parameter of 9.126 Å is expected for FeSb₃, a value that is in clear disagreement with the much larger 9.2383(6) Å found herein at 300 K. The thermal expansion calculated from the temperature dependence of the lattice parameters is shown in Fig. 6. In order to reduce noise in the data, especially at low temperatures, the temperature dependence of the lattice parameters was first modeled with a third-order polynomial function, $a_m(T)$, see the fit lines in the top of Fig. 6. The differences between the fitted curve and the data were less than $4 \cdot 10^{-4}$ Å. The thermal expansion coefficient, α , was then obtained from the derivative $\alpha = (da_m(T)/dT)/a_m(300K)$. The thermal

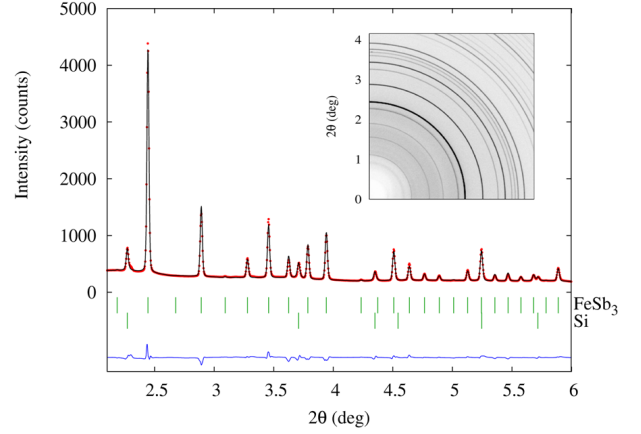


FIG. 5. X-ray diffraction pattern of FeSb₃ obtained at 10 K, red dots, the corresponding Rietveld refinement, black line, the difference plot, blue line, and the peak positions for FeSb₃ and Si, green ticks. Inset: a quarter of the corresponding detector image.

TABLE I. Rietveld refinement parameters for FeSb₃ and CoSb₃.

* constrained to the 10 K value.

	FeSb ₃ (10 K)	FeSb ₃ (300 K)	CoSb ₃ (300 K)
Bragg R-factor (%)	7	6	6
R _f (%)	6.5	6.5	5
a (Å)	9.2116(6)	9.2383(6)	9.0320(8)
y Sb	0.3402(2)	0.3399(3)	0.3356(3)
z Sb	0.1578(2)	0.1573(3)	0.1586(3)
Sb occupation (%)	0.96(1)	0.96(1)*	0.99(1)*
Density (g/cm ³)	7.157(1)	7.096(1)	7.648(1)
$\langle u^2 \rangle$ Sb (Å ²)	0.028(1)	0.034(1)	0.004(1)
$\langle u^2 \rangle$ Fe/Co (Å ²)	0.010(3)	0.013(3)	0.011(3)

expansion coefficient of CoSb₃ at 220 K, $8.8 \cdot 10^{-6} \text{ K}^{-1}$, is in good agreement with the literature value³⁵ of $9.1 \cdot 10^{-6} \text{ K}^{-1}$ as obtained from dilatometry. The thermal expansion of FeSb₃ is larger as compared with CoSb₃. Under the assumption that Poisson's ratio for CoSb₃ [9], $\nu = 0.22$, is the same for FeSb₃, the bulk modulus can be extracted from the sound velocity³⁶, which can be obtained from NIS, see below. The Grüneisen coefficient³⁷, $\gamma = 3\alpha BV_m/C_V$, can be obtained by using the thermal expansion coefficient, the bulk modulus, $B = 47.9(1)$ and $83.2(1)$ GPa for FeSb₃ and CoSb₃, respectively, the molar volume, V_m , and the heat capacity, C_V , see below. In FeSb₃ the resulting γ value of 1.4(1) at 300 K is only slightly larger than the 1.30(5) obtained for CoSb₃, because FeSb₃ exhibits both a much larger thermal expansion and a much smaller bulk modulus as compared to CoSb₃.

The isotropic mean square displacements, $\langle u^2 \rangle$, were refined for FeSb₃ and CoSb₃, see Table I. The absolute values for the Sb mean square displacements are not re-

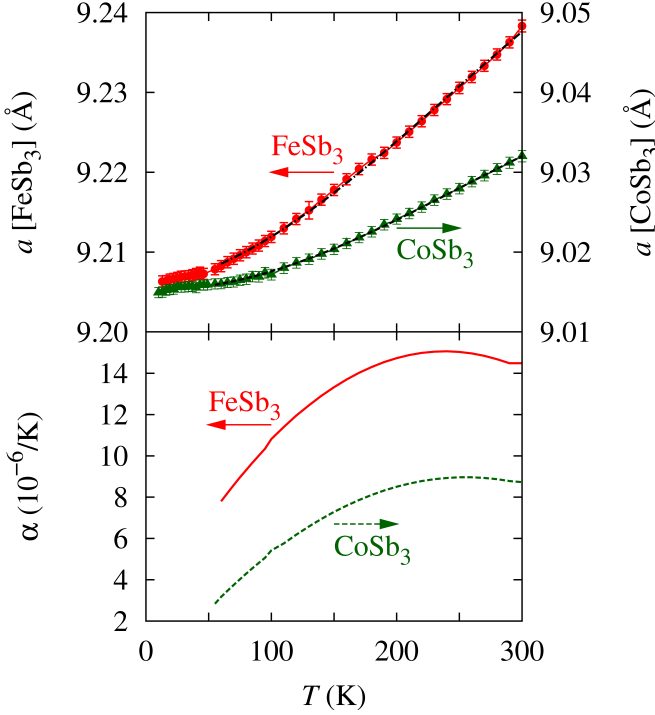


FIG. 6. The temperature dependence of the lattice parameter, a , for FeSb_3 , in red, and CoSb_3 , in green, and the corresponding polynomial fit in black, top. The thermal expansion coefficient, α , of FeSb_3 and CoSb_3 , bottom.

liable because they are too large for FeSb_3 , whereas for CoSb_3 they are too small with respect to an expected value of $\sim 0.01 \text{ \AA}^2$ at 300 K, see section III D. The reason for this discrepancy is likely that the 2θ range of the measurement was too narrow. Nevertheless, the temperature dependence of the mean square displacements is reasonable. From the slope³⁸, $d\langle u^2 \rangle/dT = 3\hbar^2/(mk_B\theta_D^2)$, where m is the mass of Sb, Fe or Co, fitted between 100 and 300 K, Debye temperatures, θ_D , of 230(5) and 410(10) K for Sb and Fe, respectively, have been obtained for FeSb_3 . The average value of the Debye temperature in FeSb_3 , calculated from $\theta_D^{av} = (3\theta_{D,\text{Sb}} + \theta_{D,\text{Fe/Co}})/4$, is 275(5) K. In CoSb_3 the Debye temperatures of 280(10) and 380(30) K for Sb and Co, respectively, have been obtained, and $\theta_D^{av} = 305(15)$ K is larger than in FeSb_3 ; the average value is in good agreement with the literature value³⁹ of 307 K, obtained from the heat capacity of CoSb_3 .

Sb is located on a general $(0, y, z)$ position and the y and z positions have been refined. The sum $y + z$ is 0.4972(6) and 0.4942(6) for FeSb_3 and CoSb_3 , respectively. FeSb_3 more closely fulfills the Oftedal relation⁴⁰, $y + z = 1/2$, which indicates that the rectangular Sb rings, see Fig. 1, are closer to squares in FeSb_3 than in CoSb_3 .

C. Mössbauer spectroscopy

The 4.2 and 295 K ^{57}Fe Mössbauer spectra of the $\sim 1.5 \mu\text{m}$ film of FeSb_3 are shown in the upper panel of Fig. 7; the spectra obtained for both films and at intermediate temperatures are very similar. In addition to the diffraction measurements that revealed no crystalline impurity phase, no further amorphous iron bearing impurity is observed. All measured spectra were fitted with a simple symmetric quadrupole doublet with two Lorentzian lineshapes, whose parameters are given in Table II. The Mössbauer spectra show no convincing evidence for a second component related to Fe with missing Sb near neighbors, as would be expected from the hypothetical partial Sb occupancy seen in the diffraction measurements. The 96(1)% Sb occupancy, see Table I, would imply that more than 20% of the Fe have less than 6 Sb near neighbors, which would be visible in the Mössbauer spectra. The temperature dependence of the isomer shift, δ , quadrupole splitting, ΔE_Q , linewidth, Γ , and the recoil-free fraction, f_{LM} , is shown in the lower portion of Fig. 7. The temperature dependence of δ and f_{LM} have been fit with a Debye model for a solid⁴¹.

The temperature dependence of the isomer shift is well fit with the Debye model⁴² for the second-order Doppler shift with a characteristic Mössbauer temperature, θ_M , of 541(10) and 530(10) K for the ~ 1.5 and $\sim 1 \mu\text{m}$ films, respectively. This temperature is much larger than the Debye temperature, $\theta_{D,\text{Fe}}$, of 350(5) and 373(6) K of the ~ 1.5 and $\sim 1 \mu\text{m}$ films, respectively, obtained from the temperature dependence of the logarithm of the spectral absorption area, f_{LM} . The latter values are in good agreement with the values obtained herein by other techniques, see Table III. It is known⁴² that the two temperatures, θ_M and $\theta_{D,\text{Fe}}$, obtained from the two temperature dependencies are usually different because they depend, for the isomer shift, on $\langle v^2 \rangle$, the mean-square vibrational velocity of the ^{57}Fe , and, for the absorption area, on $\langle u^2 \rangle$, the mean-square atomic displacement of the ^{57}Fe ; there is no model independent relationship between these mean square values⁴². However, measurements of the Mössbauer temperatures on various compounds⁴³ indicate that θ_M is often twice as large as $\theta_{D,\text{Fe}}$, i.e., the isomer shift is more sensitive to higher energy phonons.

The Fe DPS of FeSb_3 , see below, clearly reveals that the Fe vibrations have a strong non-Debye behavior and are dominated by two strong optical modes above 30 meV. Because we have measured the partial DPS, $g(E)$, by ^{57}Fe NIS, see below, we can directly obtain the second order Doppler shift⁴² $\delta_{\text{SOD}}^{g(E)} = -\langle v^2 \rangle/(2c)$ from the average kinetic energy²⁰ $\langle E_{kin} \rangle = 1/2 m_R \langle v^2 \rangle = 3/4 \int_0^\infty \coth(E/(2k_B T)) g(E) E dE$, where m_R is the mass of the resonant nucleus. The obtained temperature dependence of the isomer shift with the second order Doppler correction is shown in Fig. 7, and corresponds to $\theta_M = 440$ K. The difference is thus only partly explained and other corrections such as thermal expansion, which

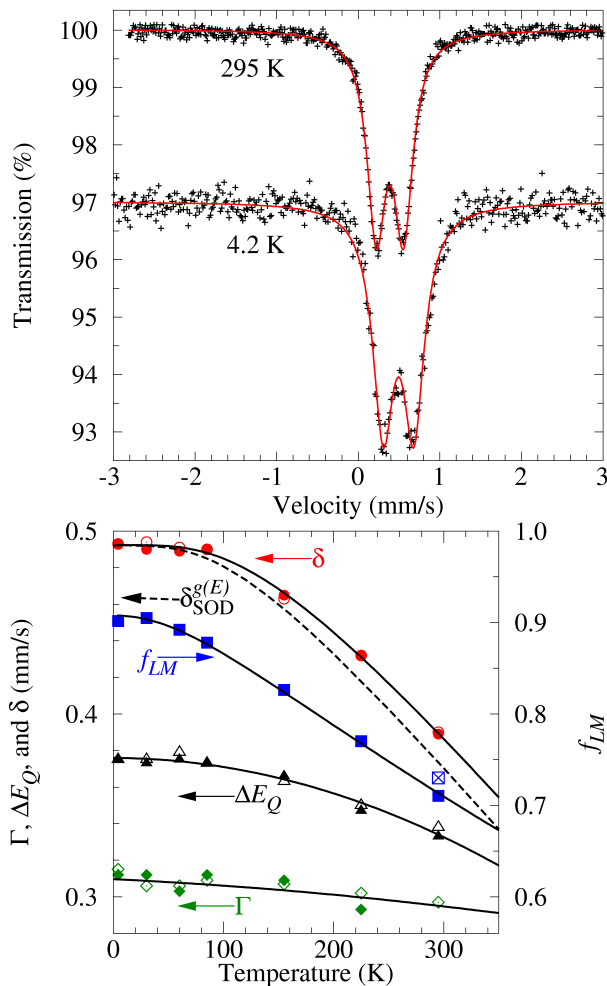


FIG. 7. Upper panel: The Mössbauer spectra of FeSb₃ obtained on a 1.5 μm film. Lower panel: The fit parameters obtained from the spectra of the ~ 1 and $\sim 1.5 \mu\text{m}$ films, open and closed symbols, respectively. The errors are the size of the symbols. The crossed square indicates the f_{LM} obtained directly from the ^{57}Fe NIS at 295 K. The dashed line indicates the second order Doppler shift obtained from the DPS, see text. The lines for the Doppler shift and f_{LM} are Debye model fits⁴¹. The lines for ΔE_Q and Γ are quadratic polynomial fits given as a guide to the eye.

modifies the DPS and therefore $\langle E_{kin} \rangle$, or the influence of charge carrier activation on the isomer shift might be necessary.

D. Nuclear resonance scattering

The nuclear inelastic scattering spectra from the ^{121}Sb NIS measurements in FeSb₃, CoSb₃, and EuFe₄Sb₁₂ are shown in Fig. 8, together with the instrumental functions measured by nuclear forward scattering. The resolution of the instrument was ~ 1.3 meV for all measurements. ^{121}Sb NIS measurements on the latter

TABLE II. Mössbauer spectral parameters for the FeSb₃ films. The errors are estimated to be 0.005 mm/s for the isomer shift, δ , quadrupole splitting, ΔE_Q , and linewidth, Γ , and 0.005 (% ϵ)(mm/s) for the absorption area.

^aThe isomer shifts are given relative to 295 K α -Fe powder.

Thickness (μm)	T (K)	δ (mm/s) ^a	ΔE_Q (mm/s)	Γ (mm/s)	Total Area (% ϵ) (mm/s)
1	295	0.390	0.338	0.297	1.668
	225	0.432	0.350	0.302	1.798
	155	0.463	0.363	0.307	1.917
	85	0.490	0.373	0.309	2.029
	60	0.491	0.379	0.306	2.037
	30	0.494	0.375	0.306	2.040
	4.2	0.493	0.375	0.315	2.070
1.5	295	0.389	0.333	0.276	2.808
	225	0.432	0.347	0.293	3.045
	155	0.465	0.366	0.309	3.266
	85	0.490	0.373	0.312	3.471
	60	0.489	0.375	0.303	3.526
	30	0.490	0.373	0.312	3.577
	4.2	0.493	0.375	0.312	3.564

two compounds have been published previously¹⁷ with a resolution of 4.5 meV. The measurements have been repeated, because of the enhanced resolution²². After subtraction of the elastic peak, the extraction of the DPS has been performed by the conventional procedure^{21,44}, *i.e.*, the correction of the multiphonon contribution of the Fourier transformation of the inelastic scattering, which was slightly modified in order to take into account the asymmetry of the instrumental function; the data were deconvoluted by the experimental instrumental function and convoluted with a symmetric Gaussian with a FWHM of 1.7 meV, a value slightly larger than the ~ 1.3 meV resolution that was chosen in order to avoid unphysical termination ripples in the DPS. The validity of the procedure was confirmed by applying the usual sum rules⁴⁵. The ^{57}Fe NIS spectrum of FeSb₃ measured at 295 K is also shown in Fig. 8. The instrumental resolution was 0.7 meV and the DPS was obtained by the conventional procedure⁴⁴. After the multiphonon correction, the partial DPS, $g(E)$, were obtained, see Fig. 9, which also shows the ^{57}Fe DPS of EuFe₄Sb₁₂ from Ref. 46. The Fe DPS consists of two small broad peaks at ~ 7 and 15 meV and a large broad peak around 30 meV. The latter broad peak is split and corresponds to a somewhat softer phonon mode in the EuFe₄Sb₁₂ filled skutterudite. The splitting of this peak was also observed in the filled skutterudite LaFe₄Sb₁₂ by inelastic neutron scattering measurements¹⁶, and in CeFe₄Sb₁₂ by NIS⁴⁶. The low energy portion of the DPS indicates that FeSb₃ is softer than EuFe₄Sb₁₂ as seen from the large increase in the reduced DPS, $g(E)/E^2$, see insets to Fig. 9. The Sb vibrations mainly appear below 25 meV, but a small contribution of the Sb vibrations is also observed around 30 meV. The latter part of the DPS is not well resolved due to the multiphonon

contributions in the experimental data. By comparing the partial DPS in different compounds, we observe that the Sb DPS in CoSb_3 exhibits pronounced features such as gaps at 12 and 21 meV and a well resolved peak at 23 meV. Inelastic neutron scattering measurements have also revealed¹⁶ this better resolution of the individual peaks in CoSb_3 as compared with $\text{RFe}_4\text{Sb}_{12}$. However, this difference is not directly related to the filling of the skutterudites, because the DPS of FeSb_3 shows the same broad features as $\text{EuFe}_4\text{Sb}_{12}$. The most pronounced difference of the DPS in FeSb_3 as compared to other filled and unfilled skutterudites is an overall softening of the phonon modes, which leads to an enhancement of the DPS between 5 and 10 meV. This softening, which is also observed in the Fe DPS in FeSb_3 at low energies, see Fig. 9, indicates a lower velocity of sound and might be crucial in determining the thermal conductivity and therefore the thermoelectric properties of skutterudites. In $\text{EuFe}_4\text{Sb}_{12}$ the essentially single frequency and Einstein like DPS of the Eu filler appears⁴⁶ at ~ 7 meV. The relative hardening of the Sb DPS between FeSb_3 and $\text{EuFe}_4\text{Sb}_{12}$, seen in the lower DPS of $\text{EuFe}_4\text{Sb}_{12}$ at ~ 7 meV, might be related to the appearance of this filler mode. Calculations of the lattice dynamics in FeSb_3 would thus be highly desirable in order to confirm this hypothesis.

Several thermodynamic and vibrational quantities can be obtained from the DPS²⁰. The element specific heat capacity, C_V , can be directly calculated from the DPS. The total heat capacity, C_V^{tot} , of FeSb_3 , obtained by combining the partial C_V for Fe and Sb obtained from NIS by $C_V^{\text{tot}} = 3 \cdot C_V^{\text{Sb}} + C_V^{\text{Fe}}$, are shown in Fig. 10. These values are compared with the total C_V of CoSb_3 , obtained by combining the partial C_V for Co from calculations¹⁶ and for Sb from NIS measurements, measurements that are in good agreement with the calculation in Ref. 16. Also a macroscopic C_P measurement of CoSb_3 , carried out with the C_P option of the QD-PPMS that is in excellent agreement with earlier results³⁹, is also shown. With a Debye fit of the C_V between 2 and 300 K, Debye temperatures for Sb and Fe in FeSb_3 of 210(5) and 430(10) K, respectively, have been obtained, values that are in good agreement with those obtained by diffraction, see Table III. From C_V^{tot} for FeSb_3 , a Debye temperature of 240(10) K has been obtained. The partial C_V of CoSb_3 yields Debye temperatures of 250(5) and 410(10) K for Sb and Co, respectively. The total Debye temperature of CoSb_3 from the macroscopic measurement is 280(10) K, in good agreement with the $\theta_D = 285(10)$ K obtained from the combined experimental ^{121}Sb NIS C_V and the theoretical Co C_V .

From the Debye level, $\lim_{E \rightarrow 0}(g(E)/E^2)$, obtained from the low energy modes in the reduced DPS, see the insets to Fig. 9, the average velocity of sound, v_s , of 2390(10) and 2790(10) m/s for FeSb_3 and $\text{EuFe}_4\text{Sb}_{12}$,

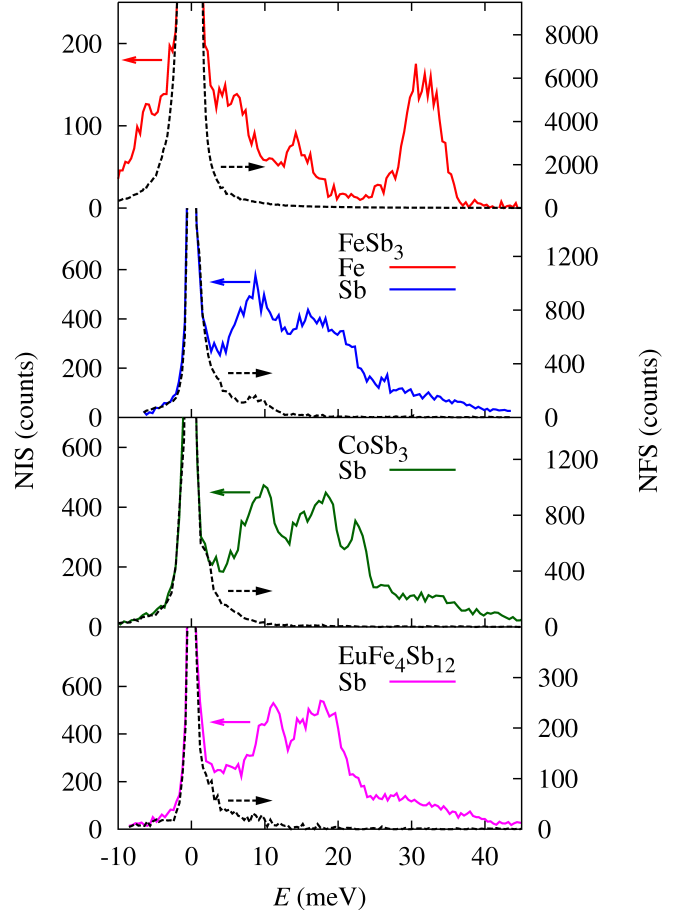


FIG. 8. The nuclear inelastic scattering, NIS, spectra and the instrumental functions, dashed lines, measured by nuclear forward scattering, NFS, obtained with the ^{57}Fe resonance of FeSb_3 , top, and with the ^{121}Sb resonance of FeSb_3 , CoSb_3 and $\text{EuFe}_4\text{Sb}_{12}$, bottom.

respectively, was obtained from the ^{57}Fe NIS by using⁴⁷

$$\lim_{E \rightarrow 0}(g(E)/E^2) = \frac{m_R}{2\pi^2 \rho \hbar^3 v_s^3} \quad (1)$$

where ρ is the density of the material and m_R the mass of the resonant nucleus. These velocities of sound are consistent with the Sb Debye level in FeSb_3 and $\text{EuFe}_4\text{Sb}_{12}$, as indicated by the dashed lines in the insets to Fig. 9, see also Table III. For CoSb_3 a v_s of 2600(100) m/s is obtained from the Debye level, in fair agreement with the literature value²⁸ of 2930 m/s. The large error arises from the imprecision in the Debye level obtained only from the ^{121}Sb NIS. By using the low temperature Debye approximation, $v_s = (k_B \theta_D)/(\hbar(6\pi^2 N)^{1/3})$, with the density of atoms N , the low temperature $\theta_D^{LT} = 245(5)$ K is obtained for FeSb_3 , a value significantly lower than $\theta_D^{LT} = 307$ K reported for CoSb_3 [39].

The Lamb-Mössbauer factor, f_{LM} , obtained from NIS provides access to the atomic mean square displacements, $\langle u^2 \rangle = -\ln(f_{LM})/k^2$, where k is the incident wavevector²⁰. In FeSb_3 the f_{LM}^{Sb} is 0.58(1) and $\langle u^2 \rangle$ is

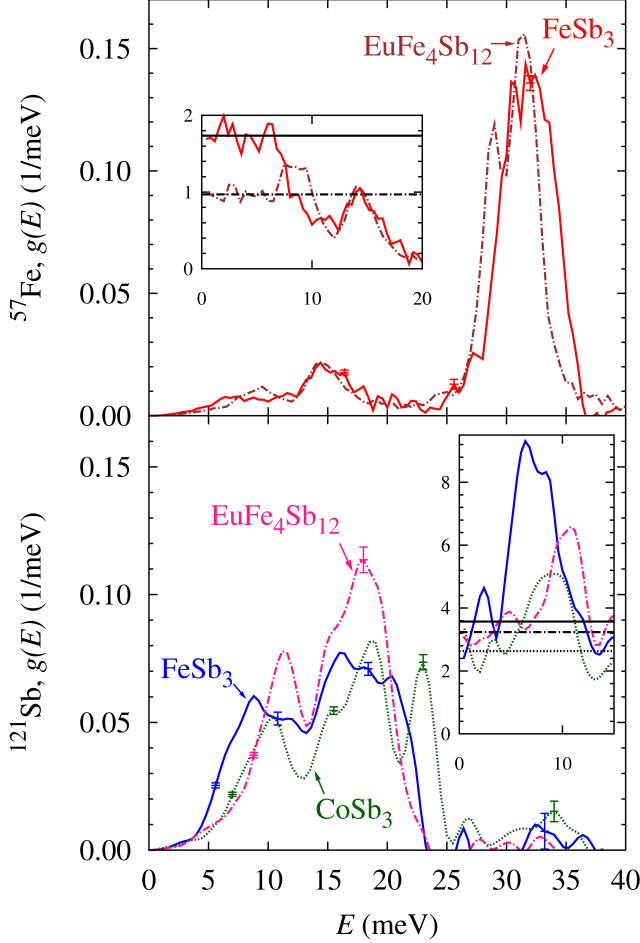


FIG. 9. Comparison of the DPS measured with the ^{57}Fe resonance at 295 K for FeSb_3 and $\text{EuFe}_4\text{Sb}_{12}$, top, and with the ^{121}Sb resonance at 25 K for FeSb_3 , CoSb_3 , and $\text{EuFe}_4\text{Sb}_{12}$, bottom. The insets show the reduced partial DPS, $g(E)/(E^2)$, in units of $10^{-4}/\text{meV}^3$ and the low energy fit, between 0 and 4 meV, for the Debye levels, indicated by the same type of lines. The differences in the Debye levels for Fe and Sb in FeSb_3 and $\text{EuFe}_4\text{Sb}_{12}$ are due to the different masses of the elements, see Eq. 1.

$0.0015(5) \text{ \AA}^2$ for Sb at 25 K and f_{LM}^{Fe} is $0.733(5)$ and $\langle u^2 \rangle$ is $0.0057(4) \text{ \AA}^2$ for Fe at 295 K. These values are much smaller than the $\langle u^2 \rangle$ values obtained by diffraction. Note that the displacement parameter obtained by NIS is a purely incoherent one particle displacement and is not affected by the site occupation or disorder as the $\langle u^2 \rangle$ values obtained from diffraction sometimes are affected. The temperature dependence of $\langle u^2 \rangle$ obtained from the DPS²⁰ is in agreement with the temperature dependence of $\langle u^2 \rangle$ obtained by diffraction, apart from an additive constant, which reflects a static displacement, or a site disorder, or an incomplete site occupation. The element specific Debye temperatures can also be calculated directly from $g(E)$ with the expres-

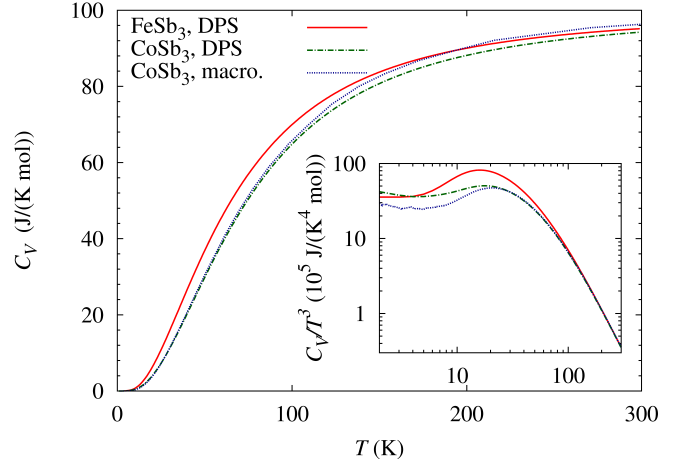


FIG. 10. A comparison of the total heat capacity, calculated from the DPS of FeSb_3 , red, the total heat capacity, calculated from the DPS and theoretical calculations for CoSb_3 , green, and the macroscopic measured heat capacity of CoSb_3 , blue.

sion $\theta_D^2 = 3/(k_B^2 \int_0^\infty g(E)dE/E^2)$ obtained in the high temperature limit, see Ref. [20]. For FeSb_3 Debye temperatures of 210(10) K for Sb and 370(5) K for Fe were obtained; the average value of 255(5) K is in agreement with 245(5) and 240(10) K obtained from sound velocity and C_V , respectively. The element specific Debye temperature in CoSb_3 was obtained from the measured ^{121}Sb DPS, 245(5) K, and from the theoretical Co DPS¹⁶, 360(10) K. In order to provide an easy comparison between the results of the different methods, we give a summary of all the Debye temperatures in Table III. Arguably, the Debye temperature is a crude approximation, but allows straightforward comparison. In essence, we observe that the Sb sublattice is systematically softer in FeSb_3 , whereas the Fe sublattice in FeSb_3 is harder than the Co sublattice in CoSb_3 .

The DPS obtained from NIS also directly yields the element specific mean force constants²⁰, $F^m = m_R/\hbar \int_0^\infty g(E)E^2 dE$. The mean force constant of 160(10) N/m for Sb in CoSb_3 is larger than the values of 105(5) and 100(10) N/m observed for FeSb_3 and $\text{EuFe}_4\text{Sb}_{12}$, respectively, because the high energy optical phonon modes of the filled structure are similar to FeSb_3 , whereas in CoSb_3 they have a larger energy. The Sb force constant in CoSb_3 deviates from the literature value of 117 N/m, obtained from earlier NIS measurements¹⁷ and 119 N/m, the mean force constant of Sb obtained from calculations¹⁶. This deviation can be ascribed essentially to the better resolution and more precise energy calibration available herein²². Thus, the good agreement obtained earlier^{16,17} is not confirmed herein and the experimental mean force constant in CoSb_3 appears to be larger than the calculated value. The Sb mean force constant for $\text{EuFe}_4\text{Sb}_{12}$ is in good agreement with the F^m

TABLE III. Summary of the Debye temperatures, sound velocities, and mean force constants in FeSb₃ and CoSb₃ obtained by different techniques.

a) obtained from $\theta_D^{av} = (3 \cdot \theta_{D,Sb} + \theta_{D,Fe/Co})/4$, b) obtained from reference [16], c) from reference [39], d) from reference [28]

Technique	FeSb ₃			CoSb ₃		
	$\theta_{D,Sb}$, K	$\theta_{D,Fe}$, K	θ_D^{av} , K	$\theta_{D,Sb}$, K	$\theta_{D,Co}$, K	θ_D^{av} , K
$\langle u^2 \rangle$, XRD	230(5)	410(10)	275(5) ^a	280(10)	380(30)	305(15) ^a
Mössbauer spectral area 1.5 μ m	-	350(5)	-	-	-	-
Heat capacity DPS	210(5)	430(10)	240(10)	250(5)	410(10) ^b	285(10)
Heat capacity macroscopic	-	-	-	-	-	280(10)
DPS	210(10)	370(5)	255(5) ^a	245(5)	360(10) ^b	270(10) ^a
θ_D from v_s	-	-	245(5)	-	-	307 ^c
	$v_{s,Sb}$, m/s	$v_{s,Fe}$, m/s	v_s^{av} , m/s	$v_{s,Sb}$, m/s	$v_{s,Co}$, m/s	v_s^{av} , m/s
NIS, Debye level	2400(100)	2390(10)	-	2600(100)	-	-
Pulse echo	-	-	-	-	-	2930 ^d
	F_{Sb}^m , N/m	F_{Fe}^m , N/m		F_{Sb}^m , N/m	F_{Co}^m , N/m	
NIS	105(5)	186(1)	-	160(10)	-	-
Theory	-	-	-	119 ^b	176 ^b	-

obtained from previous NIS measurements¹⁷. This indicates that by filling FeSb₃ with Eu, the average Sb binding does not change. Further, CoSb₃ has very different Sb lattice dynamics and thus is not an ideal compound for investigating the influence of filling upon the lattice dynamics of the RFe_4Sb_{12} compounds. In FeSb₃ the Fe

mean force constant is 186(1) N/m, a value close to the value of 190(4) N/m in EuFe₄Sb₁₂. The calculated mean force constant¹⁶ for Co in CoSb₃ of 176 N/m is slightly smaller, indicating a softer Co binding in the [Co₄Sb₁₂] framework as compared to the Fe binding in the [Fe₄Sb₁₂] framework.

IV. CONCLUSION

The magnetic and electric properties of FeSb₃ reveal semiconducting and paramagnetic behavior similar to CoSb₃, with however a larger effective paramagnetic moment. **X-ray diffraction and Mössbauer spectral measurements reveal that the sample is very pure with at most 3 weight % of elemental Sb as an impurity.** Measurements of the lattice dynamics and the related quantities show that the Sb binding in FeSb₃ is significantly softer than in CoSb₃, whereas the Fe sublattice in FeSb₃ is harder compared to the Co sublattice in CoSb₃. The softening of the low energy modes likely has a large influence on the thermal conductivity and thus favorably impacts the thermoelectric properties in FeSb₃. By filling the [Fe₄Sb₁₂] framework, the low energy optical phonon modes, which have mainly Sb character, shift to larger energies. The lattice dynamics in filled skutterudites depends both on the framework and the filler and therefore the [Co₄Sb₁₂] framework is not ideal to study the influence of the filler on the lattice dynamics in RFe_4Sb_{12} skutterudites. It appears that for skutterudites, as was also suggested for clathrates⁴⁸, the role of the framework on the lattice dynamics should be revisited.

ACKNOWLEDGMENTS

We thank Dr. H.-C. Wille and Mr. D. Bessas for their support during the NIS measurements and Dr. J.C. Feldman for making his calculation data¹⁶ available. We thank Dr. B.C. Sales for providing the CoSb₃ and EuFe₄Sb₁₂ samples¹⁷. The European Synchrotron Radiation Facility and the Advanced Photon Source are acknowledged for provision of synchrotron radiation beam time at the nuclear resonance station ID18 and ID22N and the high energy station 6-ID-D, respectively. RH acknowledges support from the Helmholtz-University Young Investigator Group 'Lattices Dynamics in Emerging Functional Materials'. FG acknowledges the financial support of the Fonds National de la Recherche Scientifique, Belgium (grants 9.456595 and 1.5.064.05). The research at the University of Oregon was funded by National Science Foundation under grant DMR 0907049 and supported in part by ONR Grant No. N00014-07-1-0358 and by the Army Research Laboratory under agreement number W911NF-07-2-0083.

-
- * r.hermann@fz-juelich.de
- ¹ J. P. Fleurial *et al.*, Thirteenth International Conference on Thermoelectrics, AIP Conference Proceedings **316**, 40-44 (1995).
 - ² B. C. Sales *et al.*, Phys. Rev. B **56**, 15081-15089 (1997).
 - ³ G. S. Nolas, D. T. Morelli, and T. M. Tritt, Annu. Rev. Mater. Sci. **29**, 89-116 (1999).
 - ⁴ C. Uher, Semiconductors and Semimetals **69**, 139-253 (2001).
 - ⁵ G. S. Nolas *et al.*, J. Appl. Phys. **79**, 4002-4008 (1995).
 - ⁶ G. S. Nolas, J. L. Cohn, and G. A. Slack, Phys. Rev. B **58**, 164-170 (1998).
 - ⁷ G. P. Meisner *et al.*, Phys. Rev. Lett. **80**, 3551-3554 (1998).
 - ⁸ J. L. Feldman, and D. J. Singh, Phys. Rev. B **53**, 6273-6282 (1996).
 - ⁹ V. Keppens *et al.*, Nature **395**, 876-878 (1998).
 - ¹⁰ R. P. Hermann *et al.*, Phys. Rev. Lett. **90**, 135505 (2003).
 - ¹¹ M. M. Koza *et al.*, Nature Materials **7**, 805-810 (2008).
 - ¹² M. Rotter *et al.*, Phys. Rev. B **77**, 144301 (2008).
 - ¹³ B. C. Sales, B. C. Chakoumakos, and D. Mandrus, Phys. Rev. B **61**, 2475-2481 (2000).
 - ¹⁴ C. Uher, *Thermoelectrics Handbook: Macro to Nano* (Taylor & Francis Group, LLC, 2006).
 - ¹⁵ J. Yang *et al.*, Phys. Rev. B **80**, 115329 (2009).
 - ¹⁶ J. L. Feldman *et al.*, Phys. Rev. B **73**, 014306 (2006).
 - ¹⁷ H. C. Wille *et al.*, Phys. Rev. B **76**, 140301(R) (2007).
 - ¹⁸ M. D. Hornbostel *et al.*, J. Am. Chem. Soc. **119**, 2665-2668 (1997).
 - ¹⁹ J. R. Williams, M. B. Johnson, and D. C. Johnson, J. Am. Chem. Soc. **123**, 1645-1649 (2001).
 - ²⁰ R. Rüffer, and A. I. Chumakov, Hyp. Interact. **128**, 225-272 (2000).
 - ²¹ W. Sturhahn *et al.*, Phys. Rev. Lett. **74**, 3832-3835 (1995).
 - ²² I. Sergueev *et al.*, J. Synch. Rad., under review (2011).
 - ²³ M. Noh, J. Thiel, and D. C. Johnson, Science **270**, 1181-1184 (1995).
 - ²⁴ A. P. Hammersley, *ESRF Internal Report, ESRF97HA02T*, 'FIT2D: An Introduction and Overview', (1997).
 - ²⁵ J. Rodriguez-Carvajal, *FULLPROF V (2009)* (Laboratoire Leon Brillouin (CEA-CNRS), France, 2009).
 - ²⁶ D. Mandrus *et al.*, Phys. Rev. B **52**, 4926-4931 (1995).
 - ²⁷ H. Anno *et al.*, J. Appl. Phys. **83**, 5270-5276 (1998).
 - ²⁸ T. Caillat, A. Borshchevsky, and J. P. Fleurial, J. Appl. Phys. **80**, 4442-4449 (1996).
 - ²⁹ L. D. Chen *et al.*, J. Appl. Phys. **90**, 1864 (2001).
 - ³⁰ M. Puyet *et al.*, Phys. Rev. B **73**, 035126 (2006).
 - ³¹ A. L. E. Smalley, S. Kim, and D. C. Johnson, Chem. Mater. **15**, 3847-3851 (2003).
 - ³² J. Yang *et al.*, Phys. Rev. B **63**, 014410 (2000).
 - ³³ J. Yang, M. G. Endres, and G. P. Meisner, Phys. Rev. B **66**, 014436 (2002).
 - ³⁴ T. Rosenqvist, Acta Metallurgica **1**, 761-763 (1953).
 - ³⁵ G. Rogl *et al.*, J. Appl. Phys. **107**, 043507 (2010).
 - ³⁶ L. Zhang *et al.*, Mat. Sci. Eng. B **170**, 26-31 (2010).
 - ³⁷ D. T. Morelli, V. Jovovic, and J. P. Heremans, Phys. Rev. Lett. **101**, 035901 (2008).
 - ³⁸ B. T. M. Willis and A.W. Pryor, *Thermal Vibrations in Crystallography* (Cambridge University Press, 1975).
 - ³⁹ R. P. Hermann, F. Grandjean, and G. J. Long, Am. J. Phys. **73**, 110-118 (2005).
 - ⁴⁰ B. C. Chakoumakos, and B. C. Sales, J. Alloys Compd. **407**, 87-93 (2006).
 - ⁴¹ R. H. Herber in *Chemical Mössbauer Spectroscopy*, edited by R. H. Herber, p.199 (Plenum Press New York, 1984).
 - ⁴² G. K. Shenoy and F. E. Wagner, *Mössbauer Isomer Shifts*, p.49 (North-Holland, Amsterdam, 1978).
 - ⁴³ T. Owen *et al.*, Inorg. Chem. **47**, 8704-8713 (2008).
 - ⁴⁴ V. G. Kohn, and A. I. Chumakov, Hyp. Interact. **125**, 205-221 (2000).
 - ⁴⁵ H. J. Lipkin, Phys. Rev. B **52**, 10073 (1995).
 - ⁴⁶ G. J. Long *et al.*, Phys. Rev. B **71**, 040302 (2005).
 - ⁴⁷ M. Y. Hu *et al.*, Phys. Rev. B **67**, 094304 (2003).
 - ⁴⁸ M. Christensen *et al.*, J. Am. Chem. Soc. **128**, 15657-15665 (2006).